



OPEN

Generation of orbital angular momentum modes via holographic leaky-wave metasurfaces

Homayoon Oraizi[✉] & Hedieh Emamian

Recently, electromagnetic (EM) waves carrying orbital angular momentum (OAM) has received considerable attention in increasingly many different realms, such as communication systems, super-resolution imaging, optical communications and quantum state manipulation. In this paper, two different kinds of two dimensional (2-D) holographic leaky-wave metasurfaces with a single OAM mode at a single frequency (18 GHz) are introduced through designs and experiments. The classic leaky-wave and a microwave holography theorem are combined to construct the holographic leaky-wave metasurfaces. The leaky wave metasurfaces-based holographic concept are implemented with isotropic artificial surface impedances and made of hexagonal metallic patches. By varying the size of the metallic patches, the effective impedances may be realized. The monopole launchers are utilized for the excitation of TM surface mode, whereby their wave functions can be approximated by the Hankel function of the second kind. The objective waves represented by the desired beams carrying different orbital angular momentum modes. Electromagnetic full-wave simulations and experimental measurements have been performed to substantiate the proposed method.

Wireless communication systems have gradually used innovative methods to meet the requirements of increased channel capacity and boost the transmission data-rate to develop communication applications. Conventional communication methods have faced the barriers of radio spectrum efficiency and the channel capacity expansion. One recently way to achieve higher capacities¹ is to spatially multiplex multiple orthogonal modes using a single transmitter/receiver aperture pair, in which each mode carries an independent data stream. Orthogonality assures that the modes can be efficiently multiplexed at the transmitter, spatially co-propagated, and are demultiplexed at the receiver with minimal modal crosstalk². As a new degree of freedom, due to the mutual orthogonality among eigenstates of the orbital angular momentum, scholars have conducted several versatile researches on the orbital angular momentum (OAM). Since then, beams carrying OAM inspires a new thinking in many diverse applications ranging from classical and quantum communication to optical manipulation³⁻⁵.

Similar to light beams, it is well-known that electromagnetic (EM) waves can carry both linear momentum (LM) and angular momentum (AM). The linear momentum of EM waves is associated with the Poynting's vector. The angular momentum constitutes spin angular momentum (SAM) and orbital angular momentum (OAM)⁶ in the paraxial regime. The SAM defines the spin feature of photon and is associated with the polarization of the light and modes of EM waves. In the optical regime, it has only two value of $\pm h$ (Planck's constant divided by 2π) per photon. In electromagnetics, three possible polarization modes may be attributed to the electromagnetic beam, namely the left- and right-circularly polarized modes and linearly polarized mode. These modes merely impose channel limitation in communication systems. On the other hand, OAM defines the orbital rotation of photon. Each photon has an OAM of $\pm lh$, where l is known as a topological charge or OAM index, which can be any integer ranging from $-\infty$ to ∞ .

In 1992⁷, Allen *et al.* first demonstrated that light beams with an azimuthal phase distribution $\exp(il\varphi)$ carries an angular momentum independent of the polarization photon state, where φ is the azimuthal angle around the propagation axis and l is the topological charge, which represents the number of twists of the wavefront. Before that, Soskin *et al.* created a structured light with helical wavefront by using forked gratings⁸. It has been used to demonstrate high-capacity optical and radio communication channels by employing multiple OAM states into the transmitted EM wave on the light. In 2007 Bo Thide introduced the OAM concept from an optical frequency to a radio band by using circular array antennas with a gradient phase difference⁹.

School of Electrical Engineering, Iran University of Science and Technology, 1684613114, Tehran, Iran. ✉e-mail: h_oraizi@iust.ac.ir

At present, various methods for generating EM OAM waves have been presented. In optics, computer-generated holograms (CGH)¹⁰, spiral phase plates (SPP)¹¹, spatial light modulators (SML)¹² and Q-plate have been generated by the spin-orbit coupling in inhomogeneous media¹³. At radio domain, circular phase array antennas^{14,15}, dielectric resonator antennas¹⁶, reflect and transmit arrays^{17,18} and metasurfaces^{19–21} have been designed. Although there are various designs in different configurations, the design principles for OAM generation lead to one universal rule: the introduction of the azimuthal phase term $\exp(il\varphi)$ to EM waves.

By comparison with the conventional methods, owing to the extreme controls of EM waves, (namely low loss, low profile, low cost, and high performance), it has been proved that metasurfaces are more convenient to create versatile radiation beams²². Generally, metasurfaces, which are the planar version of bulky 3D metamaterials are divided into two categories including periodic and quasi-periodic structures. The first category is widely used in frequency selective structures²³, polarization convertors²⁴ and polarization rotators²⁵. Meantime, much attention has been focused on the quasi-periodic structures, by reason of providing more design freedom to perform inhomogeneous surfaces. Various prototypes of radiators have been proposed for OAM generation, such as golden nanorods in²⁶, L-shaped gold nanoantennas²⁷, artificial perfect-electric and perfect-magnetic conductors anisotropic metasurface²⁸, ultra-thin complementary metasurface aimed for double-layer complementary metasurface for OAM generation with high efficiency and metasurface Fork gratings²⁹.

It is necessary to provide a more appropriate and efficient design procedure. The metasurfaces shaped by artificial impedance surfaces have many applications in designing leaky-wave antennas³⁰. Surface wave leakage manipulation is one of the important applications of metasurface³¹. Wave leakage can be made by perturbation in the propagation medium. The great advantage of the leaky-wave systems is controlling the amplitude and propagation direction of the leaky waves³². Combining with the microwave holography principle, the desired wave can be generated by exciting the hologram interference of the reference wave and object wave in any desired direction³³. The physical equivalence between the leaky waves and holographic antennas based on the Oliner's method was given in³⁴. The holography principle in optics was first introduced by Gabor³⁵. Checcacci³⁶ then utilized it at microwave frequencies. Since it has high potentials in various applications, research has been undertaken extensively on this theory. Sievenpiper³⁷ proposed the hologram leaky wave for pattern synthetization. Periodic ground patches supporting TM_0 surface wave are used to realize this concept. The new degree of freedom, which is the possibility of polarization manipulation has been added to hologram designs using anisotropic unit-cells³⁸.

In this paper, we propose two different kinds of holographic leaky-wave metasurfaces to generate OAM modes with $l = 2$ and $l = 3$ at 18 GHz. The metasurfaces comprise of hexagonal patches on the grounded dielectric. We use the monopole antenna to excite the interferogram, which is the recorded interference of reference and object waves for the generation of the desired OAM beams.

The principle of holography for designing the leaky-wave metasurface

The evolution of the holography concept, which was indicated as a two-step imaging process, opened a new vision into wave phenomena and leading to development of a new class of antenna named holographic antenna³⁹. It is important to explain the two-step imaging process, including the hologram formation and wave front reconstruction steps. Based on the microwave holographic theory, the reference wave excites the hologram and is consistent with the wave scattered from the object, which is called object wave. The intervention of the reference wave and object wave is called the interferogram pattern⁴⁰. The desired radiation waves can be generated by exciting the hologram interference (generated by the reference wave and object wave). Holographic leaky wave metasurfaces are assembled of quasi-periodic surface impedance. If (ψ_{ref}) and (ψ_{obj}) define the reference wave and object waves, respectively, the surface impedance realizing the object wave is given by:

$$Z_s = jX_0\eta_0(1 + M \times \mathcal{R}\{\psi_{ref}\psi_{obj}^*\}) \quad (1)$$

where X_0 is the normalized impedance with respect to the free space intrinsic impedance (η_0), M is the modulation depth coefficient, \mathcal{R} defines the real part of the $(\psi_{ref}\psi_{obj}^*)$ and “*” denotes the complex conjugation operation. The reference wave may be selected as the surface or space wave. Here, for our proposed metasurfaces, the reference waves are defined as cylindrical waves in the form of Hankel function of the second kind:

$$\psi_{ref} = \alpha H_0^{(2)}\left(\beta\sqrt{x^2 + y^2}\right) \quad (2)$$

where β is the phase constant for the TM_0 surface mode and is obtained as

$$\beta = k_0\sqrt{1 + X_0^2} \quad (3)$$

Observe that β is an approximation of the wave number which is applied for the object wave calculation and derivation of the associated surface impedance. The modulation factor (M) should be small value to justify the approximated value of β . Otherwise, if the modulation depth is not small, the phase constant (β) may be obtained by the dispersion relation. The desired object wave (radiation wave) in this work in a specific direction is represented as:

$$\psi_{obj} = e^{-j(kx\sin\theta_0\cos\varphi_0 + kysin\theta_0\sin\varphi_0 + l\phi)} \quad (4)$$

where θ_0 and φ_0 are the main lobe direction angles in the XZ and XY planes, respectively. l is the topological charge and defines the number of twists.

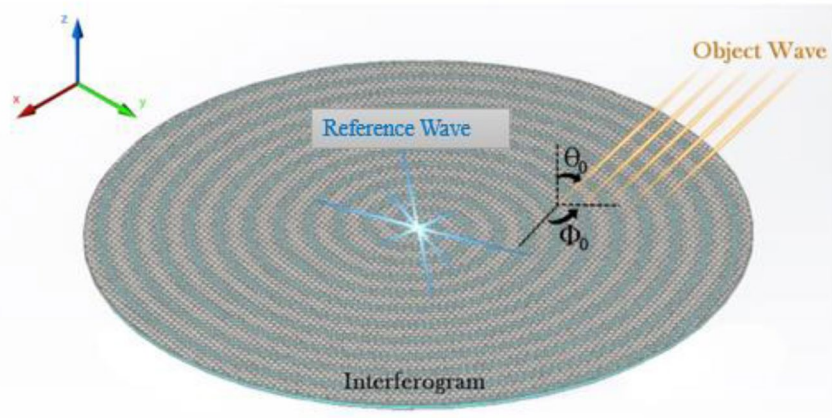


Figure 1. The schematic views of the cylindrical reference wave, object wave and interferogram.

The schematics in Fig. 1 demonstrate the hologram principle and leaky wave theory to design the holographic leaky-wave metasurface. It illustrates that exciting the interferogram or holographic surface impedance by the reference wave, the object wave or desired radiation wave is generated.

Higher-order bessel beam and orbital angular momentum

Non-diffracting Bessel beams are a set of solutions⁴¹ of the free space Helmholtz equation and have transverse intensity profiles that can be described by the Bessel function of the first kind. They have several features, such as non-diffraction, self-reconstruction, and even providing optical pulling forces. The scalar form of Bessel beams wave-function can be introduced as:

$$E(r, \varphi, z) = A \cdot \exp(ik_z z) \cdot J_n(k_r r) \cdot \exp(\pm jn\varphi) \tag{5}$$

where A is the amplitude, k_z and k_r are the corresponding transverse and longitudinal propagation constants that satisfy the equation $\sqrt{k_z^2 + k_r^2} = k = 2\pi/\lambda'$. It can be derived from Eq. (5) that the transverse intensity profiles of Bessel beams are independent of z coordinate which gives rise to their non-diffracting characteristic. Due to that OAM is structured beam with phase term $\exp(il\varphi)$ and is related to vorticity and phase singularity it also shows that any higher-order Bessel beam ($n \neq 0$) must carry an orbital angular momentum and have zero intensity along the z axis at $r = 0$ because of the phase singularity resulting from $\exp(\pm jn\varphi)$ term.

The general form of the aperture field for the Bessel beams which carry an orbital angular momentum with the mode of $(n + 1)$ can be defined as:

$$\vec{E}(r, \varphi, z) = (E_r \hat{r} + E_\varphi \hat{\phi} + E_z \hat{z}) \cdot e^{-jk_z z} e^{-j(n+1)\varphi} \tag{6}$$

$E_r, E_\varphi,$ and E_z components are:

$$\begin{pmatrix} \left(-C_{TE} \frac{J_n(k_r r) + J_{n+2}(k_r r)}{2} + i \cdot C_{TM} e^{in\eta} \sqrt{1 - NA^2} \frac{J_n(k_r r) + J_{n+2}(k_r r)}{2} \right) \hat{r} \\ - \left(C_{TM} e^{in\eta} \sqrt{1 - NA^2} \frac{J_n(k_r r) + J_{n+2}(k_r r)}{2} + i \cdot C_{TE} \frac{J_n(k_r r) + J_{n+2}(k_r r)}{2} \right) \hat{\phi} \\ NA \cdot C_{TM} e^{in\eta} J_{n+1}(k_r r) \hat{z} \end{pmatrix} \tag{7}$$

where C_{TM} and C_{TE} are complex numbers associated with the constituent transverse magnetic and transverse electric waves of Bessel beams; η is the phase difference between C_{TM} and C_{TE} . The coefficient of NA shows the contribution of z component in the near field. For high NA Bessel beams, the electric field of the z component results from TM waves: the higher the NA , the higher the contribution the TM waves make to E_z . The E_r and E_φ components mainly result from TE wave contribution, as the term $\sqrt{1 - NA^2}$ is relatively small for the high NA case.

Now consider that the value of $k_r r$ is large enough, so the argument of Bessel function can be approximated as:

$$J_n(k_r r) \approx \sqrt{\frac{2}{\pi k_r r}} \cos\left(k_r r - \frac{\pi}{4} - \frac{n\pi}{2}\right) \tag{8}$$

So $J_n(k_r r)$ and $J_{n+2}(k_r r)$ cancel each other due to a π phase difference, and the φ component of the aperture will be zero. These coefficients also have direct contributions in the far field pattern, and their effects will be canceled

in the far field. As a result, in the far field approximation, by using isotropic unit-cells we can generate OAM modes.

Analysis of monopole launcher as a reference wave

Choosing the proper reference wave is the crucial step of the design procedure of modulated metasurfaces. The monopole launcher on a grounded dielectric medium is selected for the excitation of TM_0 surface waves. The electric and magnetic fields of the monopole launcher can be defined as⁴²:

$$\vec{E}_{sw} = \left[jX_s J_{sw} H_1^{(2)}(\beta_{sw} \rho) \hat{\rho} + J_{sw} \frac{\beta_{sw} \eta_0}{k_0} H_0^{(2)}(\beta_{sw} \rho) \hat{z} \right] e^{-\alpha_z z} \quad (9)$$

$$\vec{H}_{sw} = -J_{sw} H_1^{(2)}(\beta_{sw} \rho) e^{-\alpha_z z} \hat{\phi} \quad (10)$$

where β_{sw} and α_z are the radial propagation constant and the attenuation constant in the z direction, respectively. The radial propagation constant $\beta_{sw} > k$ obeys the dispersion equation:

$$\beta_{sw} = k \sqrt{1 + \overline{X_s^2} / \eta_0^2} \quad (11)$$

$$\alpha_z = \sqrt{\beta_{sw}^2 - k^2} = \frac{k \overline{X_s}}{\eta_0} \quad (12)$$

X_s is the positive surface reactance of the grounded dielectric and TM-SW can be excited only if the reactance is positive.

It can be verified that the monopole launcher with moment $I_0 \Delta z$ have a relation with complex amplitude J_{sw} through:

$$J_{sw} = -I_0 \Delta z \frac{k_0 \beta_{sw} X_s}{2\eta_0} \quad (13)$$

The power transferred by the electric and magnetic fields is:

$$\begin{aligned} \vec{P}_{sw} = \vec{E}_{sw} \times \vec{H}_{sw}^* = -jX |J_{sw}|^2 |H_1^{(2)}(\beta_{sw} \rho)|^2 e^{-2\alpha_z z} \hat{z} + \frac{\eta_0 \beta_{sw}}{k_0} |J_{sw}|^2 H_0^{(2)}(\beta_{sw} \rho) H_1^{(2)*}(\beta_{sw} \rho) e^{-2\alpha_z z} \hat{\rho} \sqrt{b^2 - 4ac} \end{aligned} \quad (14)$$

The Poynting's vector along the ρ and z directions shows the coupling of waves to the dielectric medium. The power density cannot leave the dielectric⁴³, and the propagation only occurs along the ρ direction, because the \hat{z} component of the Poynting's vector is pure imaginary. The real part of the Poynting's vector represents the propagation along the ρ direction. Also, only this part has a contribution to the holography Eq. (1).

Holographic design of leaky-wave metasurfaces for oam beams

Figure 2a,b show the 2-D holographic interference patterns of cylindrical surface wave and desired OAM beams with the topological charge of 2 and 3, respectively. The interference patterns are signified to generate desired object waves at the direction of $\theta_0 = 0$ and $\varphi_0 = 0$. The color bar on the right shows the imaginary value of the patterns for the sample from minimum to maximum. These interferograms are extractions of the holographic equation of surface impedance (1) and the MATLAB software. For the constitution of surface impedances, it is all important that the dimensions of unit-cell be small relative to the wavelength. For the implementation of surface impedances, the grounded unit-cell patches (in the shape of square, circular, and hexagonal) are suitable.

Considering the dispersion isotropy⁴⁴, the hexagonal unit-cell is more well-behaved. Figure 3. represents the geometry of proposed unit-cell and its dispersion diagram in terms of different values of a_p . It is notable that β have direct relation with surface impedance. The variations of the dispersion diagram represent the variations of surface impedance, moreover with changing the values of a_p , the value of surface impedance changes. The value of a in Fig. 3 is 2.6 mm. The proposed method in⁴⁵ is adopted to calculate the surface impedance.

Figure 4 represents the curves of variations of imaginary parts of η_{in} and η_{surf} at frequency 18 GHz as a function of the length of the hexagonal edge (a_p). Figure 5 represents the equivalent transmission line circuit for the normal incident wave and TM mode. The surface impedance can be obtained by the conflation of the two models of transmission line in Fig. 5.

The input impedance, which is related to the reflection coefficient can be attained by a full wave simulation, which is associated with the reflection coefficient as:

$$\eta_{in} = \eta_0 \frac{1 + \Gamma}{1 - \Gamma} \quad (15)$$

We can obtain the surface impedance for the normal incidence (η_{sheet}) which is shown in Fig. 5a with the aid of Eq. (16):

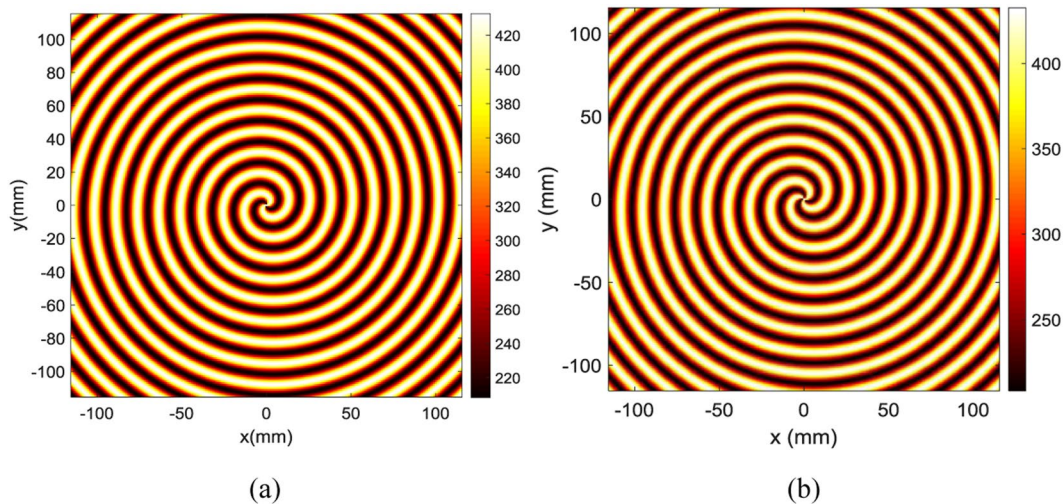


Figure 2. (a) The interference pattern of the reference wave and the object wave in direction $\theta_0 = 0$ and $\varphi_0 = 0$ for OAM mode with topological charge 2. (b) The interference pattern of the reference wave and the object wave in direction $\theta_0 = 0$ and $\varphi_0 = 0$ for OAM mode with topological charge 3.

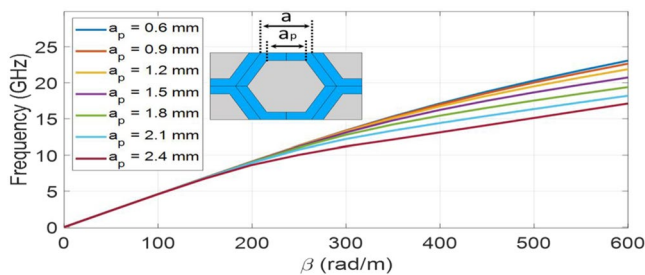


Figure 3. Geometry of the proposed unit cell and the dispersion diagram of the proposed unit-cell in terms of different values of a_p .

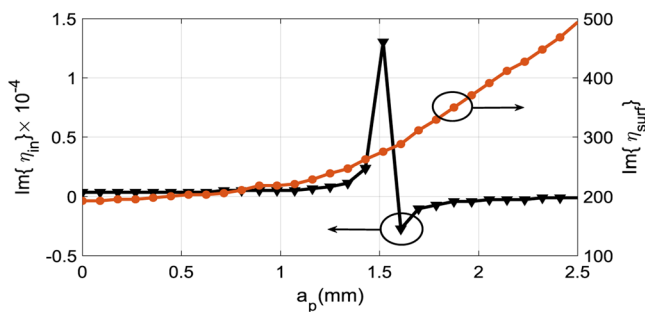


Figure 4. The curves of variations of imaginary parts of η_{in} and η_{surf} at frequency 18 GHz as a function of the length of the hexagonal edge (a_p).

$$\frac{1}{\eta_{sheet}} = \frac{1}{\eta_{in}} - \frac{1}{j\eta_1 \tan(k_1 d)} \tag{16}$$

By using η_{sheet} , the surface impedance of the incident TM mode (η_{surf}) may be obtained from the circuit in Fig. 5b:

$$\frac{1}{\eta_{surf}} = \frac{1}{\eta_{sheet}} + \frac{1}{j \frac{\eta_0 k z_1}{k_0 \epsilon_{r1}} \tan(kx_1 d)} \tag{17}$$

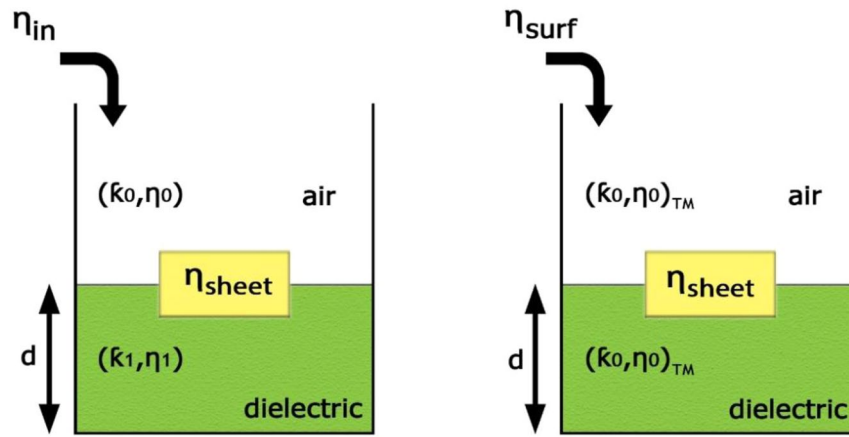


Figure 5. The equivalent transmission line of the proposed unit cell. (a) Normal incident model; (b) TM mode model.

where:

$$k_{x_1} = \sqrt{k_0^2(\epsilon_r - 1) + \left(\frac{\eta_{surf} k_0}{\eta_0}\right)^2} \tag{18}$$

As the interference patterns shown in Fig. 2a,b, two different types of holographic leaky-wave antennas are proposed for the generation of OAM modes with topological charges of $l = 2$ and $l = 3$ operating at single frequency of 18 GHz in the direction of $(\theta = 0^\circ, \varphi = 0^\circ)$, respectively. The substrate Rogers RO4003C is used in this work, which has a dielectric constant of $\epsilon_r = 3.55$, $\tan\delta = 0.0027$, and thickness of 1.524 mm. The surface impedance (comprised of different sizes of hexagonal patches) is designed to produce the desired object waves. The values of M and X_0 are arbitrary. However, their values should be selected in such a way that the impedance variation lies in the range of values obtainable by the synthesized unit-cells. Therefore, they are selected as $X_0 = 0.85$ and $M = 0.35$. When the incident electromagnetic waves (reference wave) passes through the modulated metasurfaces, the desired radiation of OAM beams are generated.

Figure 6a,b depict the shapes of the centers of the metasurfaces. Due to that the desired object waves are different, the distinctive center of metasurfaces are observable according to the figures. Note that, the surface impedance depends on the incident and object waves.

Determination of the aperture field approximation

The generalized form of the holographic theory is proposed for the synthesis of the anisotropic hologram using the aperture field approximation⁴⁶. It is proposed in this paper that for the generation of the OAM beam of mode 1, the synthesis of anisotropic surface impedances is required by the aperture field approximation.

For the generation of OAM beams, the desired object wave is represented by ψ_{obj} as an aperture electric field (\vec{E}_a):

$$\psi_{obj} = \vec{E}_a = e^{-j(\vec{k} \cdot \vec{r}) - j l \varphi} \tag{19}$$

If the aperture field is known, the antenna far-field may be calculated by⁴⁷:

$$\vec{E}(r, \theta, \varphi) = \frac{jke^{-jkr}}{2\pi r} (F_\theta(\theta, \varphi)\hat{\theta} + F_\varphi(\theta, \varphi)\hat{\varphi}) \tag{20}$$

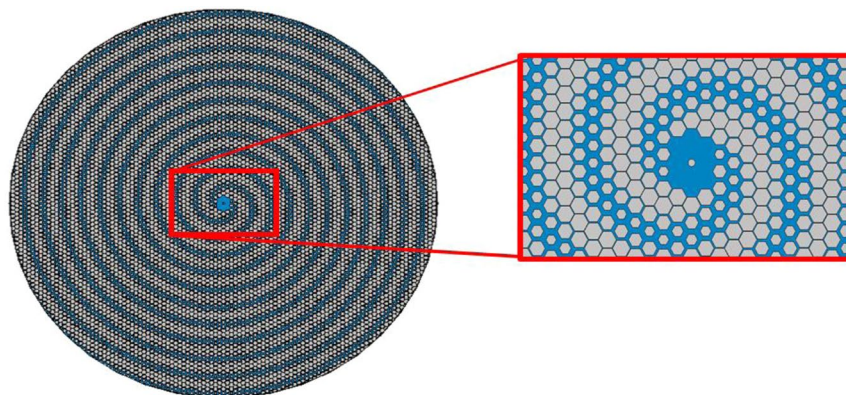
where $F_\theta(\theta, \varphi)$ and $F_\varphi(\theta, \varphi)$ are the Fourier transforms of aperture field.

$$F_\theta(\theta, \varphi) = f_x \cos \varphi + f_y \sin \varphi \tag{21}$$

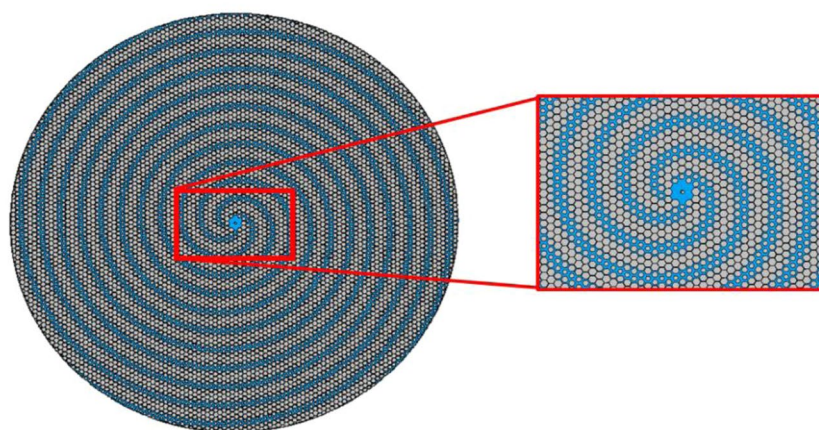
$$F_\varphi(\theta, \varphi) = \cos \theta (f_y \cos \varphi - f_x \sin \varphi) \tag{22}$$

where f_x and f_y are Fourier transforms of aperture field along the x and y axes, respectively obtained as:

$$f_x(k_x, k_y) = \int E_{ax}(\acute{x}, \acute{y}, \acute{z} = 0) e^{j(k_x \acute{x} + k_y \acute{y})} d\acute{x}d\acute{y} \tag{23}$$



(a)



(b)

Figure 6. (a) The center of Holographic Leaky-wave metasurface for OAM mode $l = 2$. (b) The center of Holographic Leaky-wave metasurface for OAM mode $l = 3$.

$$f_y(k_x, k_y) = \int E_{ay}(\acute{x}, \acute{y}, \acute{z} = 0) e^{j(k_x \acute{x} + k_y \acute{y})} d\acute{x}d\acute{y} \tag{24}$$

where E_{ax} and E_{ay} are the aperture field components in the Cartesian coordinate axes, which may be obtained by decomposing $\check{\rho} = \cos\phi\check{x} + \sin\phi\check{y}$, so:

$$\vec{E}_a = e^{-j(\vec{k} \cdot \vec{r}) - jl\phi} \check{\rho} = e^{-j(\vec{k} \cdot \vec{r}) - jl\phi} (\cos\phi\check{x} + \sin\phi\check{y}) \tag{25}$$

Substitute $\acute{x} = \rho \sin\phi$, $\acute{y} = \rho \cos\phi$, $k_x = k_0 \sin\theta \cos\phi$ and $k_y = k_0 \sin\theta \sin\phi$ into Eq. (25) to get:

$$E_{ax} = e^{-jk_0 \rho \sin\theta \cos(\phi - \phi_0) - jl\phi} \cos\phi\check{x} \tag{26}$$

$$E_{ay} = e^{-jk_0 \rho \sin\theta \cos(\phi - \phi_0) - jl\phi} \sin\phi\check{y} \tag{27}$$

Also,

$$k_x \acute{x} + k_y \acute{y} = k_0 \sin\theta \cos\phi \rho \cos\phi + k_0 \sin\theta \sin\phi \rho \sin\phi = k_0 \rho \sin\theta \cos(\phi - \phi) \tag{28}$$

By inserting Eqs. (26), (27) and (28) into Eq. (23) and (24):

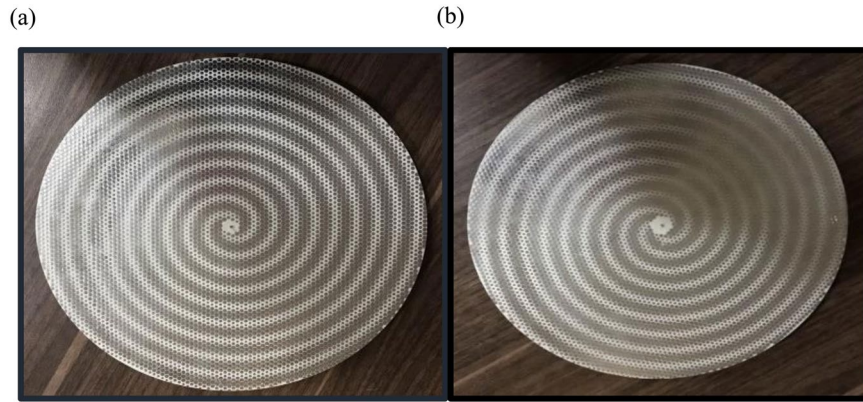


Figure 7. (a) The fabricated holographic leaky-wave metasurfaces with topological charges of OAM of $l = 2$. (b) The fabricated holographic leaky-wave metasurfaces with topological charge of OAM of $l = 3$.

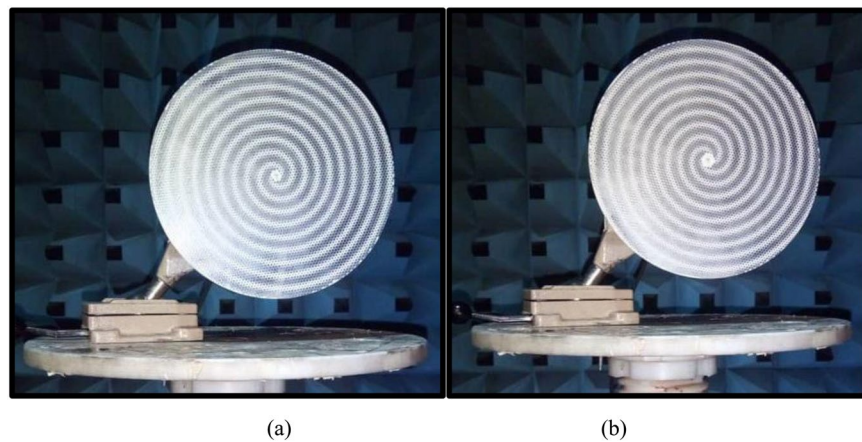


Figure 8. Experimental set-up of the proposed metasurfaces with topological charge of (a) $l = 2$ (b) $l = 3$.

$$f_x = \int_0^{2\pi} \int_0^a \cos \varphi' e^{jk_0 \rho'} (\sin \theta \cos(\varphi' - \varphi) - \sin \theta_0 \cos(\varphi' - \varphi_0)) \cdot e^{-jl\varphi} \rho' d\rho' d\varphi' \quad (29)$$

$$f_y = \int_0^{2\pi} \int_0^a \sin \varphi' e^{jk_0 \rho'} (\sin \theta \cos(\varphi' - \varphi) - \sin \theta_0 \cos(\varphi' - \varphi_0)) \cdot e^{-jl\varphi} \rho' d\rho' d\varphi' \quad (30)$$

By substituting Eqs. (29) and (30) into Eqs. (21) and (22):

$$F_\theta = \iint \cos(\varphi - \varphi_0) e^{jk_0 \rho'} (\sin \theta \cos(\varphi - \varphi_0) - \sin \theta_0 \cos(\varphi - \varphi_0)) \cdot e^{-jl\varphi} \rho' d\rho' d\varphi \quad (31)$$

$$F_\varphi = \iint \sin(\varphi - \varphi_0) e^{jk_0 \rho'} (\sin \theta \cos(\varphi - \varphi_0) - \sin \theta_0 \cos(\varphi - \varphi_0)) \cdot e^{-jl\varphi} \rho' d\rho' d\varphi \quad (32)$$

Consequently, for the isotropic structure with $l = 1$, the polarization is circular since $F_\varphi = (-j)F_\theta$. However, due to $F_\varphi \& F_\theta \neq 0$, there is no null in the pattern. Note that one of the main characteristics of the OAM beams is the existence of a null and phase singularity in the pattern. Therefore, for the generation of topological charge $l = 1$, we need to synthesize an anisotropic surface impedance.

Experimental results

As Fig. 7a,b demonstrate, the proposed holographic leaky-wave metasurfaces with different OAM modes of $l = 2$ and $l = 3$ are fabricated by using PCB technology. To vindicate our approach, the fabricated metasurfaces are measured in an anechoic chamber as shown in Fig. 8a,b. The aperture size of both metasurfaces are similar as $D = 117.75$ mm. Each element has a hexagonal lattice with a period of 2.6 mm. It is mentionable that, the distance between the unit-cells are a pivotal value for reducing the return loss (S_{11}). Also, in order to avoid spurious radiation, the hexagonal patches around the launcher are removed. Furthermore, each metasurfaces have the identical

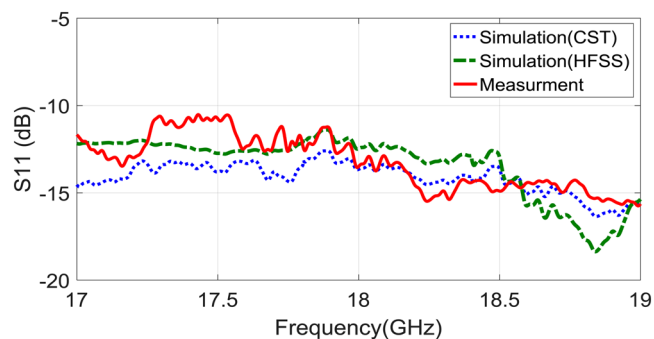


Figure 9. The simulation and measurement results for the holographic leaky-wave metasurfaces with topological charges of OAM of $l = 2$.

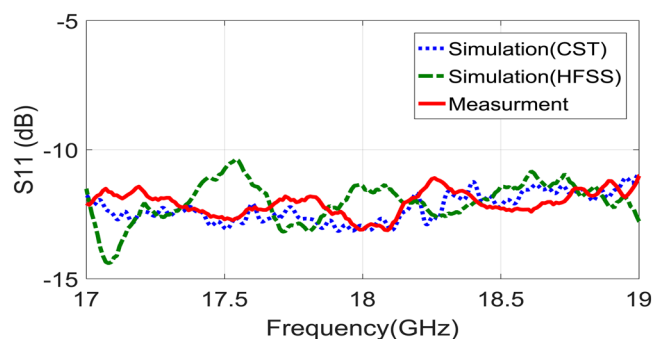
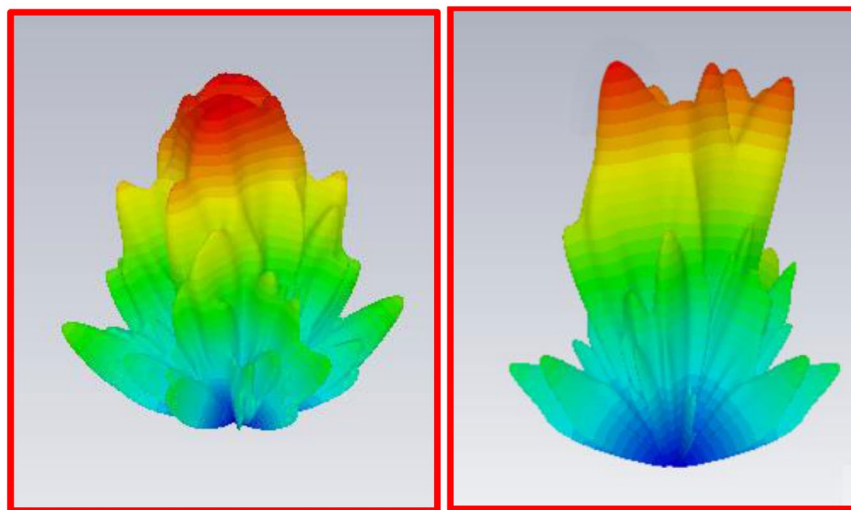


Figure 10. The simulation and measurement results for the holographic leaky-wave metasurfaces with topological charges of OAM of $l = 3$.



(a)

(b)

Figure 11. 3D far-field radiation patterns. (a) 3D far-field radiation pattern for OAM mode with $l = 2$. (b) 3D far-field radiation pattern for OAM mode with $l = 3$.

circular apertures located at the center of them. For generating reference waves, exciting the metasurfaces and impedance matching, it is essential to solder the SMA connectors behind the structures and pass them through the circular apertures. The length of the monopole was selected to be 6.724 mm (0.4λ at 18 GHz). Also, the simulations are done through CST and HFSS software by the Computer System characteristics of: CPU Core i7 6800 K/RAM: 64 GByte/Num. of Thread: 12/Num. of Cores: 6. The Figs. 9 and 10 show the simulation and

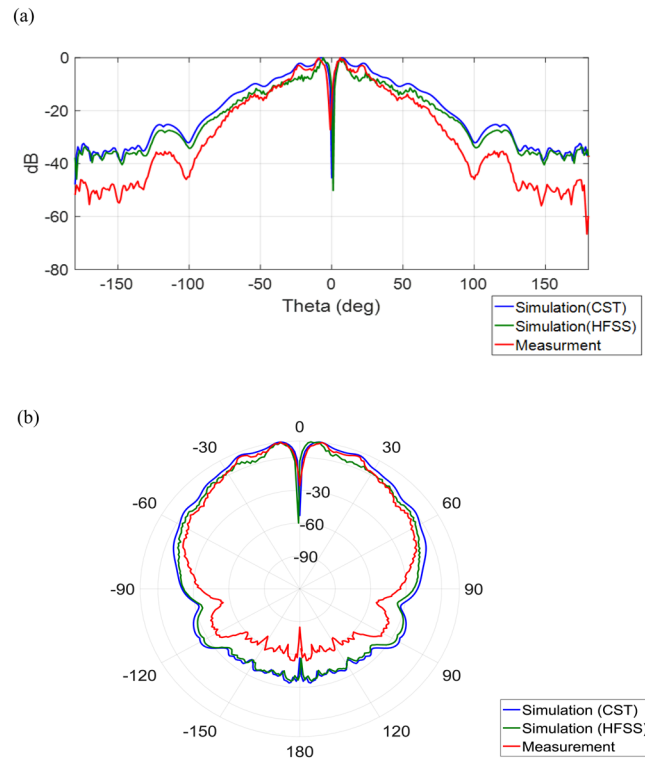


Figure 12. Simulated and measured patterns. **(a)** Simulated and measured Cartesian patterns for OAM mode with $l = 2$. **(b)** Simulated and measured polar patterns for OAM mode with $l = 2$.

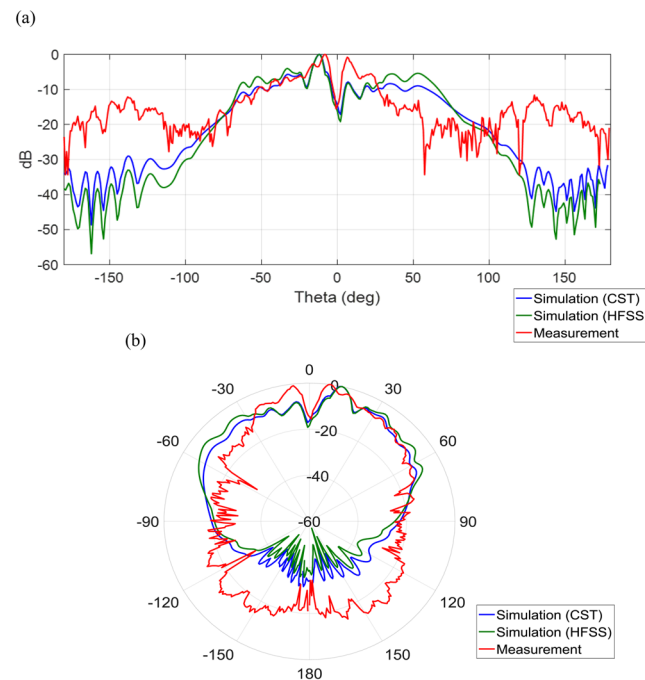


Figure 13. Simulated and Measured patterns. **(a)** Simulated and measured Cartesian patterns for OAM mode with $l = 3$. **(b)** Simulated and measurements polar patterns for OAM mode with $l = 3$.

measured reflection coefficients. The figures show that the simulated and measured values of S-parameters S_{11} are below -10 dB ranges from 17 GHz to 19 GHz.

To study the far-field radiation behavior, a standard horn antenna is located 6.5 m away from the metasurfaces. Figure 11 show the simulated 3D far-field radiation pattern. Figures 12 and 13 show the simulated and measured

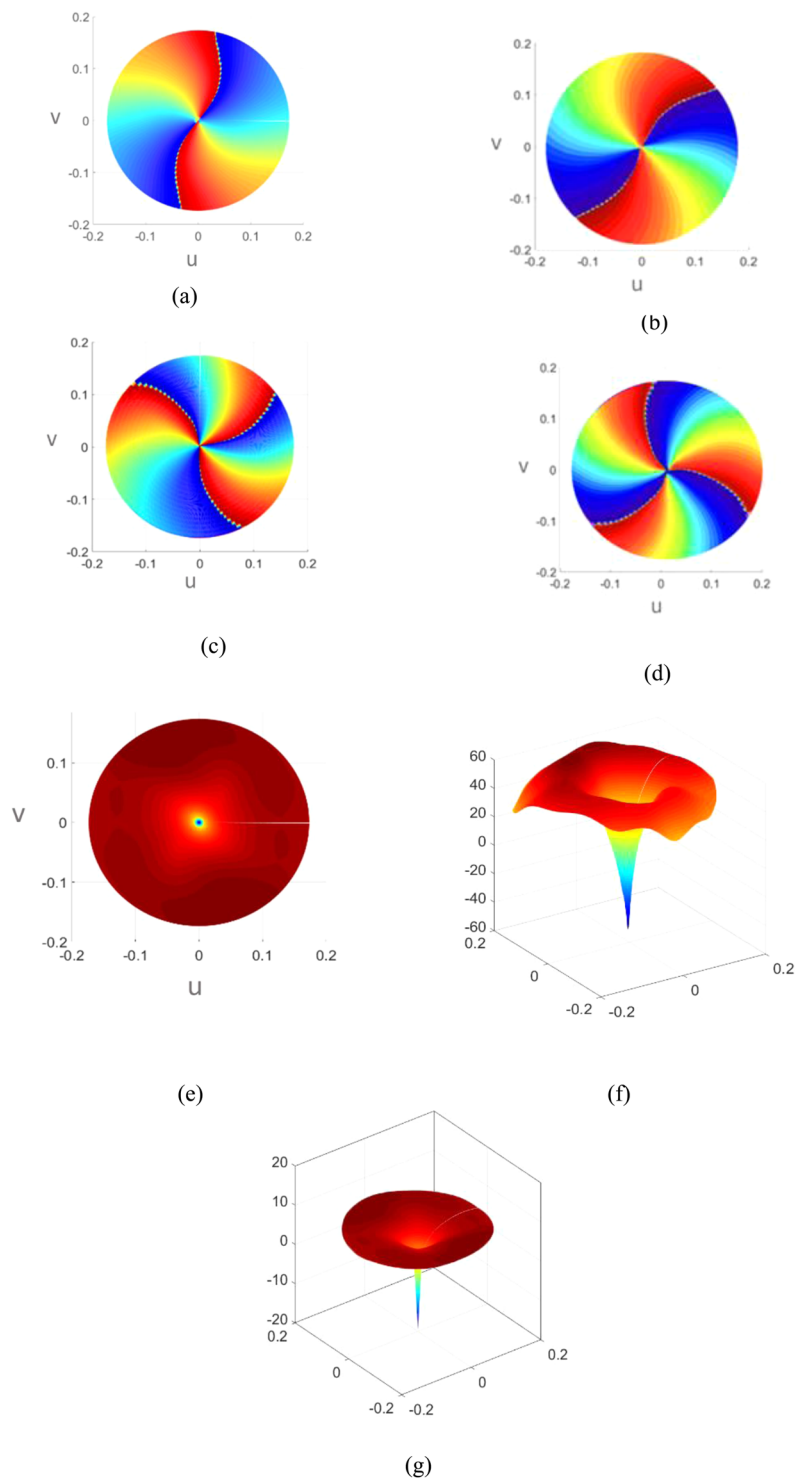


Figure 14. (a,b) The demonstration of CST and HFSS Simulation Phi-phase pattern of the holographic leaky-wave metasurfaces with topological charges of OAM of $l = 2$, respectively (c,d) The demonstration of CST and HFSS Simulation Phi-phase pattern of the holographic leaky-wave metasurfaces with topological charges of OAM of $l = 3$, respectively (e) The demonstration of CST simulation of intensity pattern of the holographic leaky-wave metasurfaces with topological charges of OAM of $l = 2$ and $l = 3$. (f,g) The demonstration of HFSS simulation of intensity pattern of the holographic leaky-wave metasurfaces with topological charges of OAM of $l = 2$ and $l = 3$, respectively.

Cartesian and polar patterns for the OAM modes. As the polar and Cartesian patterns show, there are zero depths in the desired direction, which are in accordance with the properties and features of EM OAM beams.

According to Fig. 13, the reason for the discrepancy between the simulation results and measurement data of the far-field pattern for the OAM mode 3, could be attributed to the imprecision of fabrication processes of

metasurfaces in our laboratory. Also, the measurement equipment may not have been calibrated properly for the higher order OAM modes. Note that the resolution and dimensions of the unit-cells are the limitations for synthesizing the impedance surface pattern for generating the higher order OAM modes. Also, due to the mentioned difficulties and limitations the far-field pattern of mode 3 is somewhat not symmetrical.

To verify the unique properties and features of the OAM beams, the intensity and phi-phase pattern of metasurfaces are obtained with simulations through CST and HFSS. By exporting the far-field data from the CST and HFSS and importing them to MATLAB, the data for Fig. 14 are extracted and drawn. For the figures depicting the field strength, the plots of the magnitude and phase of the far-field are drawn. Note that the vertical and the horizontal axes are in terms of $u = \sin\theta\cos\varphi$ and $v = \sin\theta\sin\varphi$, respectively.

The Fig. 14 show the phi-phase and transverse intensity pattern of the OAM beams. Observe that a clear doughnut-shaped intensity pattern appears with a singularity in the center, and a spiral-shaped phase figures show that our proposed metasurfaces significantly generate OAM modes. Also, Fig. 14f,g represent the depth of the nulls in the intensity patterns for modes of $l = 2$ and $l = 3$, where the depth of the nulls are compliance with the Figs. 12a and 13a.

Conclusion

We have successfully demonstrated two different leaky-wave metasurfaces for the generation of OAM beams. The leaky wave theory and the microwave holography method were combined to attain the interference pattern. The proposed holographic leaky-wave metasurfaces comprise of hexagonal patches which have variation in their sizes and dimensions. The patches are suitable for any direction of incident waves. We have also performed computer simulations and conducted measurements for the fabricated metasurfaces. The simulation results were in good agreement with those of experimental measurements, which strongly demonstrated the excellent performance of our design. Due to their ultralow profile, low cost, compact structure and small size and easy fabrication and integration, these metasurfaces are expected to be an effective solution for the OAM mode generations.

Received: 27 July 2019; Accepted: 13 April 2020;

Published online: 30 April 2020

References

- Demers, F., Yanikomeroğlu, H. & St-Hilaire, M. A survey of opportunities for free space optics in next generation cellular networks. Paper presented at the Ninth Annual Communication Networks and Services Research Conference (CNSR), Ottawa ON, Canada (doi: 10.1109/CNSR.2011.38) (2011, May 2–5).
- Ahmed, N. *et al.* Mode-division-multiplexing of multiple Bessel-Gaussian beams carrying orbital-angular-momentum for obstruction-tolerant free-space optical and millimetre-wave communication links. *Scientific reports* **6**, 22082 (2016).
- Grier, D. G. A revolution in optical manipulation. *Nature* **424**(no. 6950), 810–816 (2003).
- Leach, J. *et al.* Quantum correlations in optical angle-orbital angular momentum variables. *Science* **329**(no. 5592), 662–665 (2010).
- Wang, J. *et al.* Terabit free-space data transmission employing orbital angular momentum multiplexing. *Nat. Photonics* **6**(no. 7), 488–496 (2012).
- Bliokh, K. Y., Bekshaev, A. Y. & Nori, F. Dual electromagnetism: Helicity, spin, momentum and angular momentum. *New J. Phys.* **15**, 033126 (2013).
- Allen, L., Beijersbergen, M. W., Spreeuw, R. J. C. & Woerdman, J. P. Orbital Angular-Momentum of Light and the Transformation of Laguerre-Gaussian Laser Modes. *Phys. Rev. A* **45**, 8185–8189 (1992).
- Bazhenov, V. Y., Vasnetsov, M. V. & Soskin, M. S. Laser-Beams with Screw Dislocations in Their Wave-Fronts. *JETP Lett.* **52**, 429–431. (1990).
- Meng, X. *et al.* Generation of multiple beams carrying different orbital angular momentum modes based on anisotropic holographic metasurfaces in the radio-frequency domain. *Applied Physics Letters* **114**(9), 093504 (2019).
- Heckenberg, N. R., McDuff, R., Smith, C. P. & White, A. G. Generation of optical phase singularities by computer-generated holograms. *Optics Letters* **17**(3), 221–223 (1992).
- Tumbull, G. A., Robertson, D. A., Smith, G. M., Allen, L. & Padgett, M. J. The generation of free-space laguerre-gaussian modes at millimetre-wave frequencies by use of a spiral phaseplate Optical Angular Momentum, p. 186, (2003).
- Davis, J. A. *et al.* Review of operating modes for twisted nematic liquid crystal displays for applications in optical image processing. In *Optical Science and Technology*, SPIE's 48th Annual Meeting, pp. 120–131. International Society for Optics and Photonics, (2003).
- Karimi, E., Piccirillo, B., Nagali, E., Marrucci, L. & Santamato, E. Efficient generation and sorting of orbital angular momentum eigenmodes of light by thermally tuned q-plates. *Applied Physics Letters* **94**(23), 231124 (2009).
- Gao, X. *et al.* An orbital angular momentum radio communication system optimized by intensity-controlled masks effectively: Theoretical design and experimental verification. *Applied Physics Letters* **105**(no. 24), 241109 (2014).
- Gong, Y. *et al.* Generation and transmission of OAM-carrying vortex beams using circular antenna array. *IEEE Transactions on Antennas and Propagation* **65**(6), 2940–2949 (2017).
- Ren, J. & Leung, K. W. Generation of microwave orbital angular momentum states using hemispherical dielectric resonator antenna. *Applied Physics Letters* **112**(no. 13), 131103 (2018).
- Yu, S. *et al.* Design, fabrication, and measurement of reflective metasurface for orbital angular momentum vortex wave in radio frequency domain. *Applied Physics Letters* **108**(no. 12), 121903 (2016).
- Meng, X. *et al.* Generation of multiple beams carrying different orbital angular momentum modes based on anisotropic holographic metasurfaces in the radio-frequency domain. *Applied Physics Letters* **114**(no. 9), 093504 (2019).
- Zhang, K. *et al.* High efficiency metalenses with switchable functionalities in microwave region. *Applied Materials & Interfaces* **11**(31), 28423–28430, <https://doi.org/10.1021/acsami.9b07102> (2019).
- Devlin, R. C. *et al.* Spin-to-orbital angular momentum conversion in dielectric metasurfaces. *Opt. Express* **25**, 377–393 (2017).
- Yang, J. *et al.* Generation of radio vortex beams with designable polarization using anisotropic frequency selective surface. *Applied Physics Letters* **112**(no. 20), 203501 (2018).
- Karimipour, M., Komjani, N. & Aryanian, I. Shaping electromagnetic Waves with flexible and continuous control of the Beam Directions Using Holography and convolution theorem. *Scientific reports* **9**(1), 1–13. (2019).
- Wang, S.-Y., Liu, W. & Geyi, W. Dual-band transmission polarization converter based on planar-dipole pair frequency selective surface. *Sci. reports* **8**, 3791 (2018).
- Nayeri, P., Yang, F. & Elsherbini, A. Z. Design and experiment of a single-feed quad-beam reflectarray antenna. *IEEE Trans. Antennas Propag.* **60**, 1166–1171 (2012).

25. Tremain, B., Rance, H. J., Hibbins, A. P. & Sambles, J. R. Polarization conversion from a thin cavity array in the microwave regime. *Sci. reports* **5**, 9366 (2015).
26. Georgi, P., Schlickriede, C., Li, G. X., Zhang, S. & Zentgraf, T. Rotational Doppler shift induced by spin-orbit coupling of light at spinning metasurfaces. *Optica* **4**, 1000–1005 (2017).
27. Bouchard, F. *et al.* Optical spin-to-orbital angular momentum conversion in ultra-thin metasurfaces with arbitrary topological charges. *Appl. Phys. Lett.* **105**, 101905 (2014).
28. Chen, M. L. N., Jiang, L. J. & Sha, W. E. I. Artificial perfect electric conductor-perfect magnetic conductor anisotropic metasurface for generating orbital angular momentum of microwave with nearly perfect conversion efficiency. *J. Appl. Phys.* **119**, 064506 (2016).
29. Chen, S. M., Cai, Y., Li, G. X., Zhang, S. & Cheah, K. W. Geometric metasurface fork gratings for vortex-beam generation and manipulation. *Laser Photonics Rev.* **10**, 322–326 (2016).
30. Oliner, A. & Hessel, A. Guided waves on sinusoidally-modulated reactance surfaces. *IRE Transactions on Antennas and Propagation* **7**, 201–208, <https://doi.org/10.1109/TAP.1959.1144771> (1959).
31. Moeini, M. M., Oraizi, H., Amini, A. & Nayyeri, V. Wide-band beam-scanning by surface wave confinement on leaky wave holograms. *Scientific reports* **9**(1), 1–11 (2019).
32. Monticone, F. & Alù, A. Leaky-wave theory, techniques, and applications: From microwaves to visible frequencies. *Proceedings of the IEEE* **103**, 793–821, <https://doi.org/10.1109/JPROC.2015.2399419> (2015).
33. Fong, B. H., Colburn, J. S., Ottusch, J. J., Visher, J. L. & Sievenpiper, D. F. Scalar and tensor holographic artificial impedance surfaces. *IEEE Transactions on Antennas and Propagation* **58**, 3212–3221, <https://doi.org/10.1109/TAP.2010.2055812> (2010).
34. Patel, A. M. & Grbic, A. A printed leaky-wave antenna based on a sinusoidally-modulated reactance surface. *IEEE Transactions on Antennas and Propagation* **59**, 2087–2096, <https://doi.org/10.1109/TAP.2011.2143668> (2011).
35. Gabor, D. A new microscopic principle. *Nature* **161**, 777–778 (1948).
36. Checcacci, P. F., Russo, V. & Scheggi, A. M. Holographic antennas. *Proceedings of the IEEE* **56**, 2165–2167, <https://doi.org/10.1109/PROC.1968.6832> (1968).
37. Li, Y. B., Cai, B. G., Cheng, Q. & Cui, T. J. Isotropic holographic metasurfaces for dual-functional radiations without mutual interferences. *Advanced Functional Materials* **26**, 29–35, <https://doi.org/10.1002/adfm.201503654>.
38. Minatti, G., Caminita, F., Martini, E., Sabbadini, M. & Maci, S. Synthesis of modulated-metasurface antennas with amplitude, phase, and polarization control. *IEEE Transactions on Antennas and Propagation* **64**, 3907–3919, <https://doi.org/10.1109/TAP.2016.2589969> (2016).
39. Liu, D., Cheng, B., Pan, X. & Qiao, L. A horn-fed frequency scanning holographic antenna based on generalized law of reflection. *Sci. reports* **6**, 31338 (2016).
40. Hariharan, P. Basics of interferometry. 1 (Elsevier, 2007).
41. Chen, W. *et al.* Generation of wavelength-independent subwavelength Bessel beams using metasurfaces. *Light: Science & Applications* **6**(no. 5), e16259 (2017).
42. Elliot, R. *Antenna Theory and Design*, Revised Ed (Wiley India Pvt. Limited, 2006).
43. Li, M., Xiao, S. Q. & Sievenpiper, D. F. Polarization-insensitive holographic surfaces with broadside radiation. *IEEE Transactions on Antennas and Propagation* **64**, 5272–5280, <https://doi.org/10.1109/TAP.2016.2618853> (2016).
44. Oraizi, H., Amini, A., Abdolali, A. & Karimimehr, M. Design of wideband leaky wave antenna using sinusoidally modulated impedance surface based on the holography theory. *IEEE Antennas and Wireless Propagation Letters* **1–1**, <https://doi.org/10.1109/LAWP.2018.2866712> (2018).
45. Pandi, S., Balanis, C. A. & Birtcher, C. R. Analysis of wideband multilayered sinusoidally modulated metasurface. *IEEE Antennas and Wireless Propagation Letters* **15**, 1491–1494, <https://doi.org/10.1109/LAWP.2015.2514241> (2016).
46. Minatti, G. *et al.* Modulated metasurface antennas for space: Synthesis, analysis and realizations. *IEEE Transactions on Antennas and Propagation* **63**(4), 1288–1300 (April 2015).
47. Balanis, C. A. *Antenna Theory: Analysis and Design*. (Wiley, Inc., 4th ed., 2016).

Author contributions

H.O. proposed the method. H.E. developed the method, did the simulations and set up the experiments. H.O. analyzed the results and supervised the project. H.O. wrote the main manuscript text. All authors discussed the results and commented on the manuscript.

Competing interests

The authors declare no competing interests.

Additional information

Correspondence and requests for materials should be addressed to H.O.

Reprints and permissions information is available at www.nature.com/reprints.

Publisher's note Springer Nature remains neutral with regard to jurisdictional claims in published maps and institutional affiliations.



Open Access This article is licensed under a Creative Commons Attribution 4.0 International License, which permits use, sharing, adaptation, distribution and reproduction in any medium or format, as long as you give appropriate credit to the original author(s) and the source, provide a link to the Creative Commons license, and indicate if changes were made. The images or other third party material in this article are included in the article's Creative Commons license, unless indicated otherwise in a credit line to the material. If material is not included in the article's Creative Commons license and your intended use is not permitted by statutory regulation or exceeds the permitted use, you will need to obtain permission directly from the copyright holder. To view a copy of this license, visit <http://creativecommons.org/licenses/by/4.0/>.

© The Author(s) 2020